

# Communication

## Detecting Step Edges in Noisy SAR Images: A New Linear Operator

Philippe Paillou

**Abstract**—We present in this communication a new linear edge detector that is very well suited to process noisy images. Performances of the new operator have been evaluated using Canny's criteria together with experimental comparison results on a noisy SAR image.

### I. INTRODUCTION

A critical step for computer image processing is the edge-detection process. Edges are associated with intensity changes in the image and are efficient descriptors of the image structure. Results of the edge-detection process are used in higher level image analysis stages such as pattern recognition and three dimensional (3-D) reconstruction [12], [17]. An edge detector should satisfy several criteria: low sensitivity to noise, good edge localization, and no false edges detection [1].

Several operators were developed such as, for instance, morphological edge detectors [9]–[11] and differentiation-based edge detectors [2]–[4], [8], [13], [15], [16]. The latter are mainly based on either detection of maxima of the gradient or zero crossings of the second derivatives. A pre-processing smoothing step is often needed as differential operators are sensitive to noise. In particular, when considering synthetic aperture radar (SAR) images, now widely used for remote sensing [5]–[7], noise is a crucial point. In order to be able to efficiently detect edges in such images, one should consider an operator with very low sensitivity to noise.

We propose in this communication a new linear edge detector that has such a property. This operator was derived from Deriche filter [3], [4] and can be recursively implemented. We first present the new filter in Section II, and compare it to commonly used edge detectors. Section III describes the recursive realization of the filter in the two-dimensional (2-D) case. Experimental results on a synthetic test image and on a real SAR image from SIR-C mission are presented in Section IV. The proposed operator shows better performance in insensibility to noise compared to other operators; this new filter can be of great help in processing noisy SAR images.

### II. A NEW LINEAR EDGE DETECTOR

#### A. Filter Presentation

Let us consider a 1D noisy edge  $S(x)$  as

$$S(x) = A \frac{d}{dx} \delta(x) + n(x) \quad (1)$$

with  $A$  a constant,  $\delta(x)$  the Dirac distribution, and  $n(x)$  some white noise. In fact, all edges are not only step edges (see [14], for instance) and noise in SAR images presents a Rayleigh distribution.

Edge detection is performed by convoluting the noisy step edge with an antisymmetrical function  $f(x)$ . The edge is located at maxima

Manuscript received November 29, 1995; revised February 16, 1996.

The author is with the Institut de Géodynamique, Université de Bordeaux, F-33405 Talence Cedex, France.

Publisher Item Identifier S 0196-2892(97)00970-4.

of the result of convolution  $O(x_o)$  given by

$$O(x_o) = \int_{-\infty}^{+\infty} S(x) f(x_o - x) dx. \quad (2)$$

Canny [1] defined the following three quality criteria, to be maximized by the operator  $f(x)$ .

1) *Insensibility to noise:*

$$\Sigma = \int_{-\infty}^0 f(x) dx \Big/ \sqrt{\int_{-\infty}^{+\infty} f^2(x) dx}. \quad (3)$$

2) *Good edge localization:*

$$\lambda = |f'(0)| \Big/ \sqrt{\int_{-\infty}^{+\infty} f'^2(x) dx}. \quad (4)$$

3) *Unique response to one edge:*

$$k = |f'(0)| \Big/ \left( \sum \sqrt{\int_{-\infty}^{+\infty} f''^2(x) dx} \right). \quad (5)$$

Deriche [3] used Canny's criteria to derive an optimal operator

$$f_D(x) = -c \exp(-\alpha|x|) \sin(\omega x), \quad c > 0, \alpha > 0, \omega > 0 \quad (6)$$

for which quality criteria are

$$\Sigma_D = \sqrt{\frac{2}{\alpha(1+q^2)}}, \quad \lambda_D = \sqrt{2\alpha}, \quad k_D = \sqrt{\frac{1+q^2}{5+q^2}} \quad \text{with } q = \frac{\omega}{\alpha} < 1. \quad (7)$$

We propose here to use a dual form of Deriche operator, that is an hyperbolic sinus form expressed by

$$f_P(x) = -c \exp(-\alpha|x|) \sinh(\omega x), \quad c > 0, \alpha > 0, \omega > 0 \quad (8)$$

for which quality criteria are

$$\Sigma_P = \sqrt{\frac{2}{\alpha(1-q^2)}}, \quad \lambda_P = \sqrt{2\alpha}, \quad k_P = \sqrt{\frac{1-q^2}{5-q^2}} \quad \text{with } q = \frac{\omega}{\alpha} < 1. \quad (9)$$

In fact, the localization criterion  $\lambda$  is the same for the two operators but the other criteria  $\Sigma$  and  $k$  differ: when  $q$  increases,  $\Sigma_D$  decreases and  $k_D$  increases, whereas  $\Sigma_P$  increases and  $k_P$  decreases (see Fig. 1).

This property of the new proposed filter allows to obtain high values for  $\Sigma$ , that is highly insensitive to noise, when  $q \rightarrow 1$ . Of course, a tradeoff has to be found since in that case  $k \rightarrow 0$ , and multiple edges can be generated.

#### B. Comparison with Other Edge Detectors

The previously described edge detector was compared to commonly used differential operators (including Deriche's).

1) *Canny Filter (First Derivative of a Gaussian):*

$$f_G = -cx \exp(-\alpha^2 x^2), \quad c > 0, \alpha > 0$$

$$\Sigma_G = \frac{0.89}{\sqrt{\alpha}}, \quad \lambda_G = 1.03\sqrt{\alpha}, \quad k_G = 0.52. \quad (10)$$

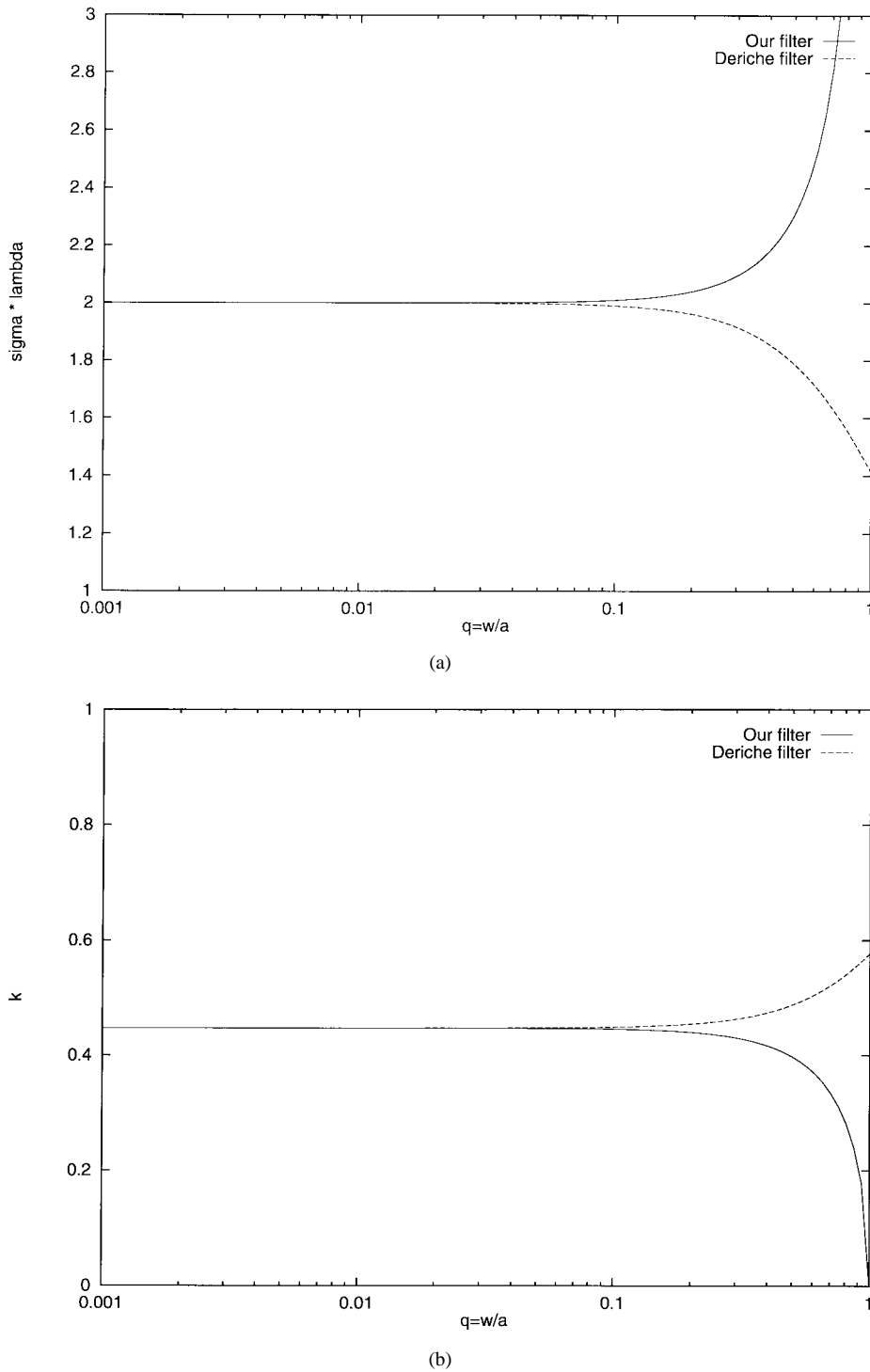


Fig. 1. (a)  $\Sigma \lambda$  and (b)  $k$  criteria as a function of  $q = \omega/\alpha$  for Deriche filter and our filter.

## 2) Shen-Castan Filter:

$$f_S(x) = -c \operatorname{sign}(x) \exp(-\alpha|x|), \quad c > 0, \alpha > 0$$

$$\sum_S = \frac{1}{\sqrt{\alpha}}, \quad \lambda_S = \infty, \quad k_S = 1. \quad (11)$$

We can see that, for a given value of parameter  $\alpha$ , the proposed filter allows the highest values for the  $\Sigma$  criterion under the condition  $\omega/\alpha \rightarrow 1$ .

This means that the new edge detector should give the best performances for noisy images, as will be shown in Section IV. It should be noted that the Shen-Castan filter presents the best possible

edge localization performance: however, this can be approached with the proposed filter by choosing a high value for the parameter  $\alpha$ .

## III. RECURSIVE IMPLEMENTATION

The proposed operator corresponds to an IIR filter that can be recursively implemented using 2-D separable masks in  $x$  and  $y$  image directions.

The  $f_p(x)$  filter  $Z$ -Transform is

$$F_P(Z) = \frac{a_1 Z^{-1}}{1 + b_1 Z^{-1} + b_2 Z^{-2}} - \frac{a_1 Z}{1 + b_1 Z + b_2 Z^2}$$

with

$$\begin{aligned} a_1 &= 2 \exp(-\alpha) \cosh(\omega) - \exp(-2\alpha) - 1 \\ b_1 &= -2 \exp(-\alpha) \cosh(\omega) \\ b_2 &= \exp(-2\alpha). \end{aligned} \quad (12)$$

The integral  $h_p(x)$  of  $f_p(x)$  is

$$h_P(x) = (c_1 \sinh(\omega|x|) + c_2 \cosh(\omega|x|)) \exp(-\alpha|x|)$$

with

$$\begin{aligned} c_1 &= \alpha d, \quad c_2 = \omega d, \\ d &= \frac{1 - 2 \exp(-\alpha) \cosh(\omega) + \exp(-2\alpha)}{2\alpha \exp(-\alpha) \sinh(\omega) + \omega(1 - \exp(-2\alpha))} \end{aligned} \quad (13)$$

and its  $Z$ -Transform is

$$H_P(Z) = \frac{a_{0p} + a_{1p}Z^{-1}}{1 + b_1Z^{-1} + b_2Z^{-2}} + \frac{a_{1m}Z + a_{2m}Z^2}{1 + b_1Z + b_2Z^2}$$

with

$$\begin{aligned} a_{0p} &= c_2 \\ a_{1p} &= (c_1 \sinh(\omega) - c_2 \cosh(\omega)) \exp(-\alpha) \\ a_{1m} &= a_{1p} - c_2 b_1 \\ a_{2m} &= -c_2 b_2. \end{aligned} \quad (14)$$

The input image  $I(i, j)$  of size  $S_x \times S_y$  is convoluted with a mask  $X(i, j)$  to obtain a first image  $I_x(i, j)$ , and is convoluted with a mask  $Y(i, j)$  to obtain a second image  $I_y(i, j)$ . The gradient amplitude image  $A(i, j)$  and the gradient direction image  $D(i, j)$  are given by the following relationships, edges being located at maxima of the gradient amplitude image

$$\begin{aligned} A(i, j) &= \sqrt{I_x^2(i, j) + I_y^2(i, j)} \\ D(i, j) &= \arctan\left(\frac{I_y(i, j)}{I_x(i, j)}\right). \end{aligned} \quad (15)$$

The  $I_x(i, j)$  image is obtained using

$$\begin{aligned} I_x(i, j) &= I_{xp}(i, j) + I_{xm}(i, j) \\ \text{with } i &= 1 \cdots S_x, j = 1 \cdots S_y \end{aligned} \quad (16)$$

$$\begin{aligned} I_{xp}(i, j) &= a_{0p}I_{x0}(i, j) + a_{1p}I_{x0}(i-1, j) - b_1I_{xp}(i-1, j) \\ &\quad - b_2I_{xp}(i-2, j) \\ \text{with } i &= 1 \cdots S_x, j = 1 \cdots S_y \end{aligned} \quad (17)$$

$$\begin{aligned} I_{xm}(i, j) &= a_{1m}I_{x0}(i+1, j) + a_{2m}I_{x0}(i+2, j) \\ &\quad - b_1I_{xm}(i+1, j) - b_2I_{xm}(i+2, j) \\ \text{with } i &= S_x \cdots 1, j = 1 \cdots S_y \end{aligned} \quad (18)$$

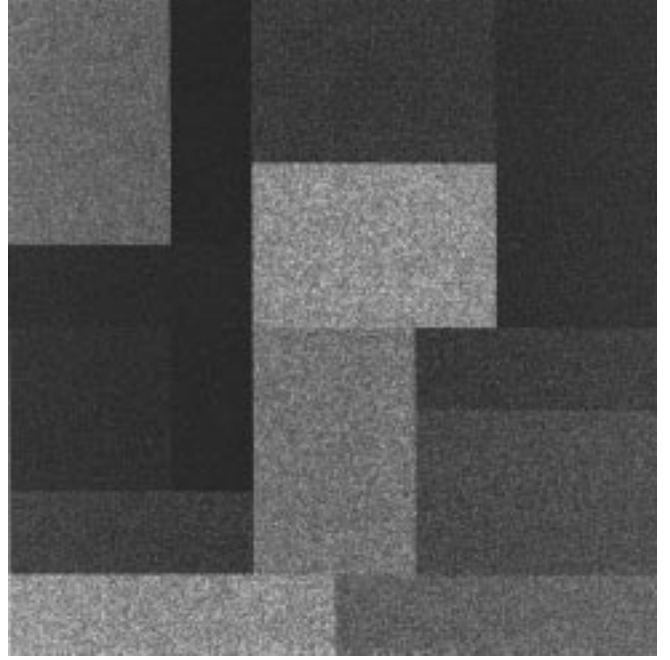
$$\begin{aligned} I_{x0}(i, j) &= a_1(X_p(i, j) - X_m(i, j)) \\ \text{with } i &= 1 \cdots S_x, j = 1 \cdots S_y \end{aligned} \quad (19)$$

$$\begin{aligned} X_p(i, j) &= I(i, j-1) - b_1X_p(i, j-1) - b_2X_p(i, j-2) \\ \text{with } i &= 1 \cdots S_x, j = 1 \cdots S_y \end{aligned} \quad (20)$$

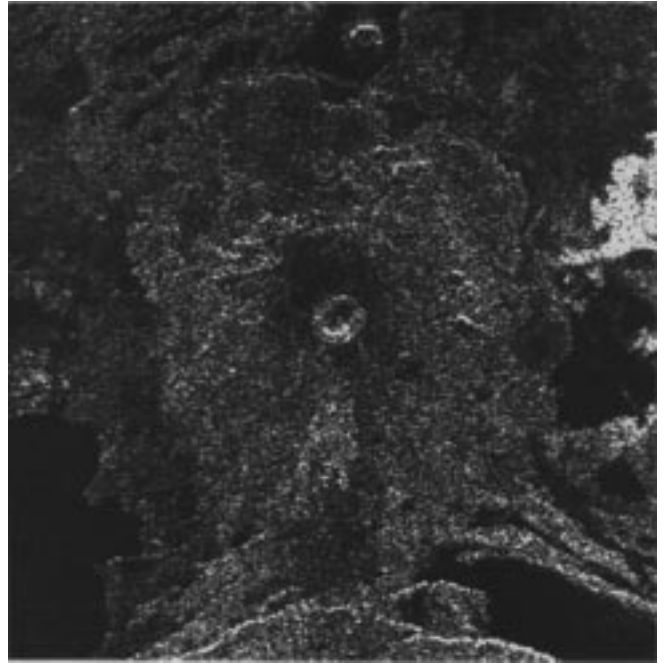
$$\begin{aligned} X_m(i, j) &= I(i, j+1) - b_1X_m(i, j+1) - b_2X_m(i, j+2) \\ \text{with } i &= 1 \cdots S_x, j = S_y \cdots 1. \end{aligned} \quad (21)$$

In a similar way, the  $I_y(i, j)$  image is obtained using

$$\begin{aligned} I_y(i, j) &= I_{yp}(i, j) + I_{ym}(i, j) \\ \text{with } i &= 1 \cdots S_x, j = 1 \cdots S_y \end{aligned} \quad (22)$$



(a)



(b)

Fig. 2. (a) Synthetic noisy image and (b) SIR-C SAR image of an Ethiopian volcano (NASA/JPL).

$$\begin{aligned} I_{yp}(i, j) &= a_{0p}I_{y0}(i, j) + a_{1p}I_{y0}(i, j-1) - b_1I_{yp}(i, j-1) \\ &\quad - b_2I_{yp}(i, j-2) \\ \text{with } i &= 1 \cdots S_x, j = 1 \cdots S_y \end{aligned} \quad (23)$$

$$\begin{aligned} I_{ym}(i, j) &= a_{1m}I_{y0}(i, j+1) + a_{2m}I_{y0}(i, j+2) \\ &\quad - b_1I_{ym}(i, j+1) - b_2I_{ym}(i, j+2) \\ \text{with } i &= 1 \cdots S_x, j = S_y \cdots 1 \end{aligned} \quad (24)$$

$$\begin{aligned} I_{y0}(i, j) &= a_1(Y_p(i, j) - Y_m(i, j)) \\ \text{with } i &= 1 \cdots S_x, j = 1 \cdots S_y \end{aligned} \quad (25)$$

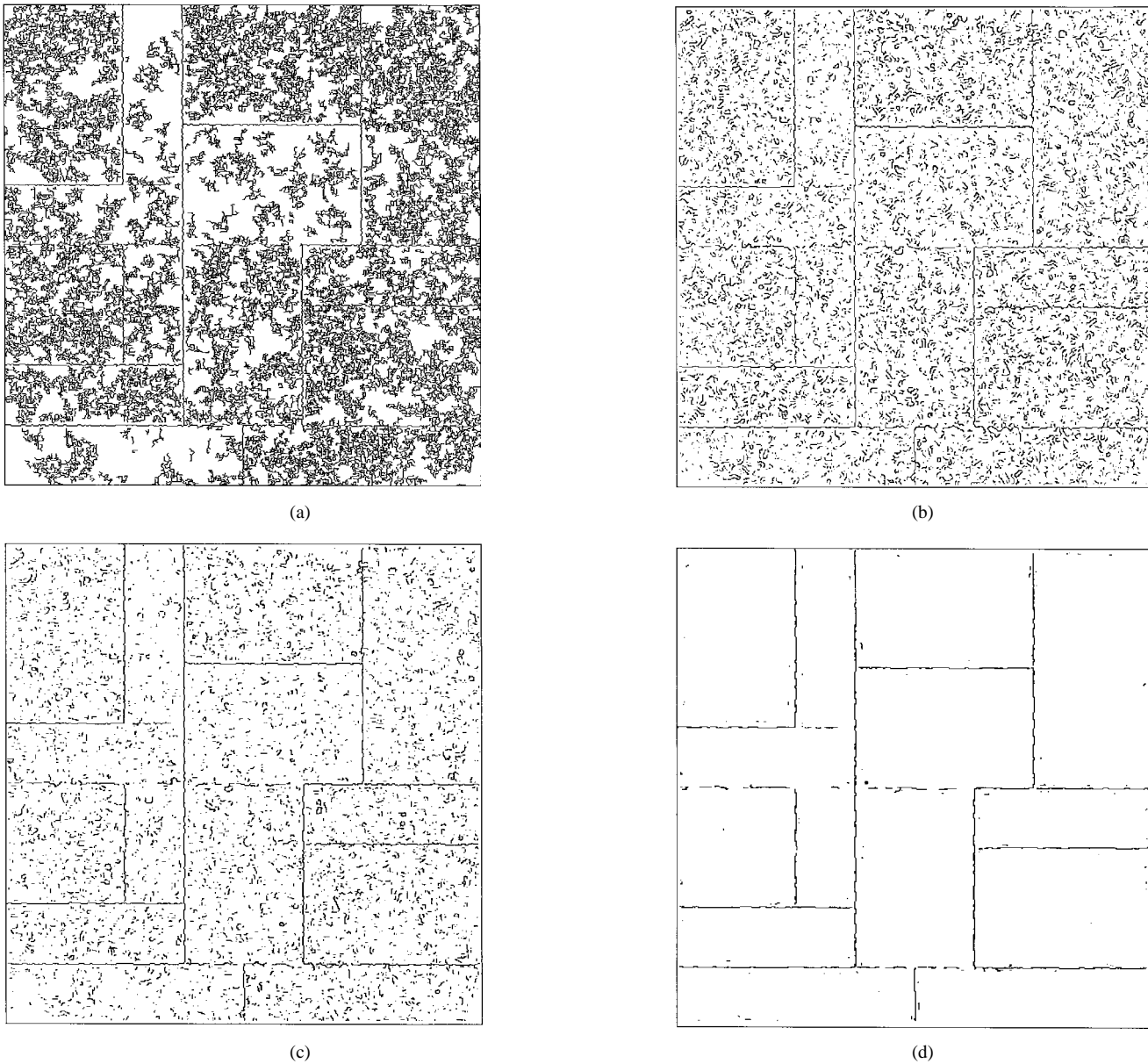


Fig. 3. (a) Results of edge detection for the synthetic image using Shen–Castan operator. (b) First derivative of a Gaussian. (c) Deriche operator. (d) The proposed filter.

$$Y_p(i, j) = I(i-1, j) - b_1 Y_p(i-1, j) - b_2 Y_p(i-2, j) \quad (26)$$

with  $i = 1 \cdots S_x, j = 1 \cdots S_y$

$$Y_m(i, j) = I(i+1, j) - b_1 Y_m(i+1, j) - b_2 Y_m(i+2, j) \quad (27)$$

with  $i = S_x \cdots 1, j = 1 \cdots S_y$ .

This recursive implementation is very efficient, since the initial image  $I(i, j)$  can be processed using only 13 multiplications and 12 additions per input pixel.

#### IV. EXPERIMENTAL RESULTS

The new linear operator was tested using a synthetic test image with white noise [see Fig. 2(a)] and using a noisy SAR image of an Ethiopian volcano obtained from the U.S. SIR-C mission [see Fig. 2(b)]. Each image is composed of  $512 \times 512$  bytes.

Fig. 3 shows results of edge detection using various operators for the synthetic test image. We set each detector parameter value in order to get the best result; that is, extract the main image structures, get as few noisy structures as possible, and avoid breaking large structure contours.

*Fig. 3(a):* Edges detected at the maxima of the gradient amplitude for symmetric exponential filter of Shen–Castan, using standard thresholding ( $\alpha = 0.45$ , threshold = 20,  $\Sigma = 1.49$ ,  $\lambda = \infty$ ,  $k = 1$ ).

*Fig. 3(b):* Edges detected at the maxima of the gradient amplitude for first derivative of a Gaussian filter, using standard thresholding ( $a = 0.5$ , threshold = 20,  $\Sigma = 1.26$ ,  $\lambda = 0.73$ ,  $k = 0.52$ ).

*Fig. 3(c):* Edges detected at the maxima of the gradient amplitude for Deriche filter, using standard thresholding ( $a = 1.0$ ,  $w = 0.01$ , threshold = 20,  $\Sigma = 1.41$ ,  $\lambda = 1.41$ ,  $k = 0.45$ ).

*Fig. 3(d):* Edges detected at the maxima of the gradient amplitude for the proposed filter, using standard thresholding ( $a = 1.0$ ,  $w = 0.7$ , threshold = 20,  $\Sigma = 1.98$ ,  $\lambda = 1.41$ ,  $k = 0.34$ ).

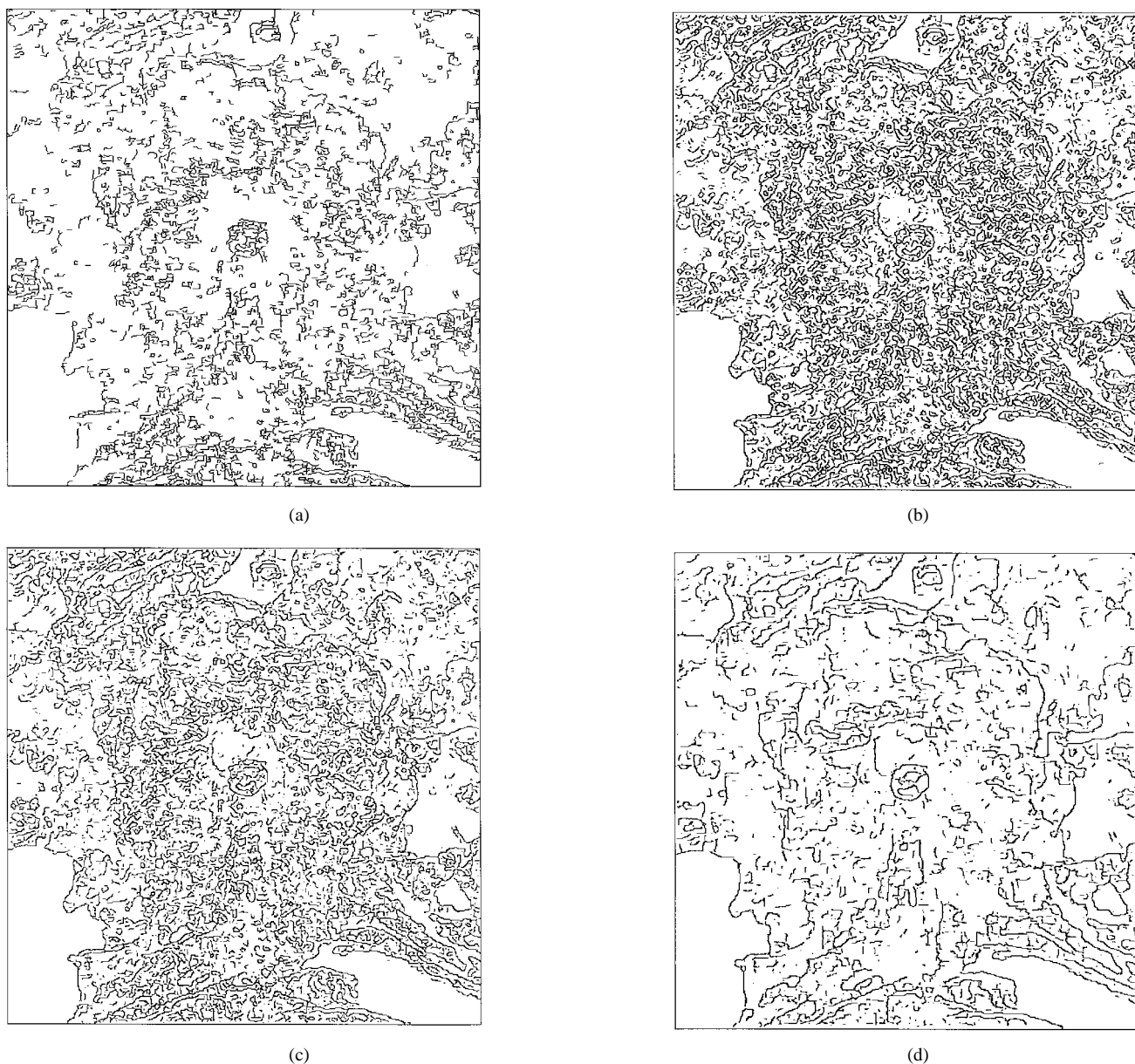


Fig. 4. (a) Results of edge detection for the SAR image using Shen-Castan operator. (b) First derivative of a Gaussian. (c) Deriche operator. (d) Proposed filter.

Fig. 3 shows that the new edge detector presents better performances with respect to insensibility to noise: the main image structures are detected well despite the noise.

Fig. 4 shows results of edge detection using the same operators and parameter values as previously for a noisy SAR image. Again, the proposed edge detector presents the best behavior: the main volcano structures are well extracted from the noise.

A new linear operator for detecting edges is presented in this communication. The filter was derived from that of Deriche and it allows us to obtain very high insensitivity to noise. It is well adapted to edge detection in noisy images such as SAR ones, and can be recursively implemented. Results obtained show better performances than those of classical differential operators.

#### REFERENCES

- [1] J. F. Canny, "Finding edges and lines in images," MIT Tech. Rep. 720, 1983.
- [2] —, "A computational approach to edge detection," *IEEE Trans. Pattern Anal. Machine Intell.*, vol. PAMI-8, 1986.
- [3] R. Deriche, "Using Canny's criteria to derive a recursively implemented optimal edge detector," *Int. J. Comput. Vision*, 1987.
- [4] —, "Fast algorithms for low-level vision," *IEEE Trans. Pattern Anal. Machine Intell.*, vol. 12, 1989.
- [5] M. C. Dobson, F. T. Ulaby, and L. E. Pierce, "Land-cover classification and estimation of terrain attributes using Synthetic Aperture Radar," *Remote Sensing Environ.*, vol. 51, pp. 199–214, 1995.
- [6] C. Elachi, *Spaceborne Radar Remote Sensing: Applications and Techniques*. New York: IEEE Press, 1987.
- [7] D. Evans, "Current status and future developments in radar remote sensing," *ISPRS J. Phot. and Remote Sensing*, vol. 47, 1992.
- [8] R. Haralick, "Digital step edges from zero-crossings of second directional derivatives," *IEEE Trans. Pattern Anal. Machine Intell.*, vol. PAMI-6, 1984.
- [9] R. J. Holyer and S. H. Peckinpaugh, "Edge detection applied to satellite imagery of the oceans," *IEEE Trans. Geosci. Remote Sensing*, vol. 27, pp. 45–56, 1989.
- [10] S. Krishnamurthy, S. S. Iyengar, R. J. Holyer, and M. Lybanon, "Histogram-based morphological edge detector," *IEEE Trans. Geosci. Remote Sensing*, vol. 32, pp. 759–767, 1994.
- [11] J. Lee, R. Haralick, and L. Shapiro, "Morphologic edge detection," *IEEE J. Robot. Automat.*, vol. RA-3, 1987.

- [12] J. Le Moigne and J. C. Tilton, "Refining image segmentation by integration of edge and region data," *IEEE Trans. Geosci. Remote Sensing*, vol. 33, pp. 605–615, 1995.
- [13] D. Marr and E. C. Hildreth, "Theory of edge detection," in *Proc. Roy. Soc. London*, vol. B207, 1980.
- [14] P. Paillou, "Non-antisymmetrical edge profile detection," *Pattern Recogn. Lett.*, vol. 15, 1994.
- [15] J. Shen and S. Castan, "An optimal linear operator for edge detection," in *Proc. CVPR'86* Miami, FL, 1986.
- [16] —, "An optimal linear operator for step edge detection," *CVGIP: GMIP*, vol. 54, 1992.
- [17] J. F. Wang, "LINDA—A system for automated linear feature detection and analysis," *Can. J. Remote Sensing*, vol. 19, 1993.

## Limitations on the Possible Resolution Enhancement of ERS-1 Scatterometer Images

N. P. Walker

**Abstract**—If methods can be devised for enhancing the spatial resolution of ERS-1 scatterometer images, then this will help to extend the range of land applications for which this data is appropriate. This paper will show that it is not possible to improve the resolution below a limit of  $\sim 25$  km.

### I. INTRODUCTION

Although the ERS-1 scatterometer was primarily designed for measuring ocean surface-wind velocities, the wide swath (500 km) and global coverage (in three to four days) offered by this instrument have also excited considerable interest for use in land and ice applications [12], [14]. However, the low spatial resolution ( $\sim 47$  km) of the scatterometer images means that it is only possible to identify large scale features.

The range of land and ice applications for which scatterometer images might be useful could be substantially increased if a significant improvement is made to the resolution of the instrument. To date, work in the area of enhancing scatterometer data has been principally conducted by Long *et al.* [6], [7], Hardin and Long [4], and Long and Hardin [8] using an algorithm which was developed for use with Seasat scatterometer (SASS) data.

The first step used by Long *et al.* to improve the resolution of the SASS scatterometer data involved taking advantage of the spatial overlap in scatterometer measurements made at different times. By combining the data from different antenna passes on a finer pixel grid, it was possible to artificially synthesize an image with a less coarse tiling effect and therefore build up a more complete picture of the ground scene. This process of combining data from different antenna passes will not, in itself, increase the resolution of the image beyond that determined by the instrument impulse response function. Instead, it can be seen as essentially a method to overcome the fact that the data from a single SASS scatterometer antenna is inadequately sampled. The second stage used by Long *et al.* involved

Manuscript received October 31, 1995; revised June 20, 1996. This work was supported as a part of an ESA study under contract 11122/94/I-HGE(SC) concerning scatterometer and radiometer land applications run by P. Lecomte at ESRIN, Italy, and in collaboration with J. Pulliainen and M. Hallikainen at the Helsinki University of Technology, Finland.

The author is with GEC-Marconi Research Centre, Chelmsford, Essex, CM2 8HN, UK (e-mail: nicholas.walker@gecm.com).

Publisher Item Identifier S 0196-2892(97)00368-9.

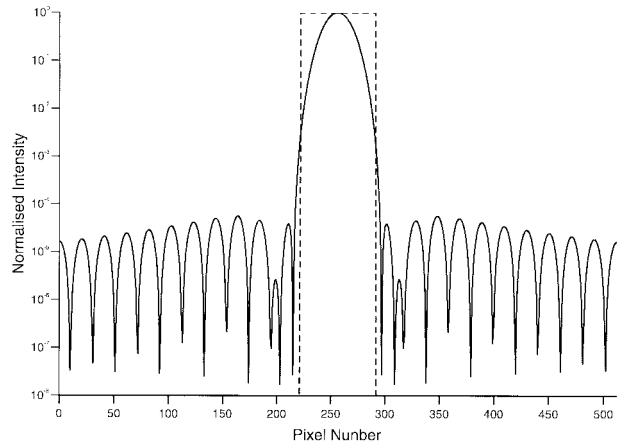


Fig. 1. The power spectrum of the Hamming window function plotted on a logarithmic scale. The dashed line indicates the sampling frequency for ERS-1 scatterometer images.

a technique referred to as multiplicative algebraic reconstruction which includes an edge preserving median filter. More recently, the enhanced resolution method due to Long *et al.* [7] has also been adapted for use with ERS-1 data Long *et al.* [9] and Early *et al.* [2].

### II. THE ERS-1 SCATTEROMETER PROCESSING CHAIN

In this section an overview is given of the aspects of the ERS-1 scatterometer processing chain which are important from the point of view of improving the spatial resolution. Further details are given in [3] and [11].

The ERS-1 wind scatterometer operates at C band with VV polarization and uses three side-looking antennae, one of which points in a direction perpendicular to the direction of flight, the other two point at  $45^\circ$  in forward and backward directions. A scatterometer image product contains  $19 \times 19$  pixels and each of these pixels represents an area of approximately  $25 \times 25$  km<sup>2</sup>. The radar cross section ( $\sigma^0$ ) value at each pixel is an average formed by a two-dimensional (2-D) weighted integration of a number of received echo signals.

Most of the ERS-1 scatterometer processing is performed on the ground. The final stage in the processing chain is a spatial averaging process which increases the radiometric resolution of the data. The spatial integration stage determines which pulses will be used to form the  $\sigma^0$  value at any given node. The integration takes place over an area which is centred on a node and is approximately 85 km square (it is 84.5 km square for the fore and aft beams and 86 km square for the mid beam [10]). The contributions of the pulses from this area are weighted by a Hamming function. The Hamming window is widely used in signal processing [5] and takes the following form

$$w(n) = \alpha + (1 - \alpha) \cos\left(\frac{2\pi}{N}n\right) \quad (1)$$

where  $|n| \leq N/2$ . By using trigonometric relations it can be shown that this equation is a cosine squared function which sits on a pedestal above the zero level. In general, the Hamming window is designed to have a Fourier transform with low sidelobes. The value of  $\alpha$  (which can vary between zero and one) used in the scatterometer weighting function is set to 0.54. This value produces the optimum level of